



Nanoscale

Observing dynamic molecular changes at single-molecule level in a cucurbituril based plasmonic molecular junction

Journal:	<i>Nanoscale</i>
Manuscript ID	NR-ART-04-2020-003360.R2
Article Type:	Paper
Date Submitted by the Author:	03-Aug-2020
Complete List of Authors:	<p>Ai, Qiushuang; Wuhan University of Science and Technology Zhou, Jianghao; Wuhan University of Science and Technology Guo, Jing; Florida International University, Physics Pandey, Popular; Florida International University Liu, Simin; Wuhan University of Science and Technology, School of chemistry and chemical engineering Fu, Qiang; Jiangxi College of Traditional Chinese Medicine Liu, Yichong; Wuhan University of Science and Technology, Deng, Chengji; Wuhan Univ Sci Technol, Chang, Shuai; Wuhan University of Science and Technology, Liang, Feng; Wuhan University of Science and Technology, He, Jin; Florida International University, Physics department</p>

SCHOLARONE™
Manuscripts

Observing dynamic molecular changes at single-molecule level in a cucurbituril based plasmonic molecular junction

Qiushuang Ai^{a,b,d+}, Jianghao Zhou^{a,d+}, Jing Guo^d, Popular Panday^d, Simin Liu^b, Qiang Fu^f, Yichong Liu^a, Chengji Deng^a, Shuai Chang^{a,c}, Feng Liang^{a,b}, Jin He^{*d,e}

In recent years, surface enhanced Raman spectroscopy (SERS) has emerged as a prominent tool for probing molecular interaction and reaction with single-molecule sensitivity. Here we use SERS to investigate the dynamic changes of the cucurbit[7]uril (CB[7]) based plasmonic molecular junctions in solution, which are spontaneously formed by the adsorption of gold nanoparticles (GNPs) at the CB[7] modified gold nanoelectrode (GNE) surface. The typical fingerprint Raman peaks of CB[7] are very weak in the SERS spectra. However, chemically enhanced peaks are prominent in the spectra due to the charge transfer across the metal-molecule interface through specific noncovalent interactions between the gold atoms and CB[7] or its guest molecule. We first investigated the selectively enhanced and greatly shifted C=O peak of CB[7] in the SERS spectra. Based on the bias-dependent changes of the C=O peak, we found the gold-carbonyl interaction was strengthened by the positive bias applied to the GNE, resulting in stable CB[7] junctions. Next, we found the CB[7] junction could also be stabilized by the inclusion of a guest molecule amino-ferrocene, attributing to the interactions between gold adatoms and the cyclopentadienyl ring of the guest molecule. Because this interaction is sensitive to the orientation of the guest molecule in the cavity, we revealed the rotational motion of guest molecule inside the CB[7] cavity based on the dynamic spectral changes of the cyclopentadienyl ring peak.

Introduction

CB[7] molecule is a barrel-shaped macrocyclic molecule with a hydrophobic inner cavity and two identical carbonyl-lined portals.¹ Various guest molecules can be included inside the CB[7] cavity through host-guest interactions. Although the individual gold-carbonyl interaction is weak, the collective interactions by multiple carbonyl groups can immobilize the CB[7] stably on the gold surface.² In recent years, surface-enhanced Raman spectroscopy (SERS) has become a promising new tool for single-molecule studies.³⁻⁵ Baumberg and Scherman pioneered the single-molecule SERS study of CB[7] and its host-guest complexes in plasmonic nanogap structures, such as “nanoparticle on mirror” (NPoM)⁶ or nanoparticle dimer^{7, 8} geometries. The plasmonic coupling between two closely spaced metal nanostructures gives rise to a highly

localized and greatly enhanced electromagnetic field in the nanogap, known as a hotspot,^{9, 10} which could effectively amplify the Raman cross sections of local molecules and enable single-molecule measurements. They have found that the CB[7] linked plasmonic nanogaps are structurally well-defined and stable because of the stable adsorption of CB[7] to the GNP surface and the rigid molecular structure of CB[7].⁷ However, the Raman signals of CB[7] are generally weak even inside a nanogap hotspot and thus the dynamics of CB[7] in the junction at the single-molecule level are difficult to be observed, especially at a few tens of microsecond time resolution.⁶

In this report, we demonstrate the dynamics of CB[7] based plasmonic junctions can be probed by utilizing unique vibrational modes of CB[7] and its guest molecule, which are chemically enhanced by the weak and reversible metal-molecule interactions. The plasmonic nanogaps of CB[7] and its host-guest complex are formed in electrolyte at room temperature by the collision of individual gold nanoparticles (GNPs) at the apex of a gold nanoelectrode (GNE) functionalized with CB[7] or its host-guest complex (Fig. 1). The stochastic collision events of GNPs at the GNE apex has been extensively investigated by the time-resolved electrochemical current measurements.¹¹⁻¹³ The self-formed “nanoparticle on nanoelectrode” (NPoNE) geometry is analogous to the NPoM.^{14, 15} However, the instability of GNPs on the highly curved GNE apex is utilized to limit the number of stably formed NPoNE structures, providing opportunities to continuously detect dynamic assembling and disassembling process of CB[7] based plasmonic molecular junctions and the associated changes at

^a The State Key Laboratory of Refractories and Metallurgy.

^b School of Chemistry and Chemical Engineering.

^c Institute of Advanced Materials and Nanotechnology, Wuhan University of Science and Technology, Wuhan, Hubei, 430081, China.

^d Department of Physics,

^e Biomolecular Science Institute, Florida International University, Miami, Florida 33199, USA

^f Jiangxi College of Traditional Chinese Medicine, Fuzhou 344000, China

† equal contribution

‡ E-mail address: schang23@wust.edu.cn, feng_liang@whu.edu.cn, jinhe@fiu.edu. Electronic Supplementary Information (ESI) available: Chemicals; The electrochemical measurements and FTIR spectra of CB[7]; The fabrication, chemical modification and characterization of GNEs; FDTD simulations; DFT calculations; The assignment of Raman vibration modes for CB[7] molecule; The SERS spectra of Citrate groups; Electrochemical current measurements; additional data

the single-molecule level.¹⁶ These dynamic changes are probed by the time-resolved SERS measurements with tens of ms time resolution. The typical CB[7] vibrational modes below 1550 cm^{-1} are very weak. Surprisingly, the peak from the vibrational mode of CB[7] carbonyl groups always appear near 2000 cm^{-1} and are greatly enhanced in the confined NPoNE structures. Density functional theory (DFT) calculations revealed the metal-to-molecule charge-transfer (CT) based chemical enhancement (CE) mechanism for the vibrational mode of carbonyl group. The shift and intensity changes of the pronounced C=O peak can be used to monitor the changes of gold-CB[7] interactions at both interfaces in the NPoNE geometry. The dynamics of guest molecule complexed in the CB[7] cavity are also probed at the single-molecule level using both the chemically enhanced fingerprint vibrational modes of guest molecule and carbonyl groups of CB[7].

Results and discussion

Fig. 1a shows a schematic layout of the experimental set up. An electrochemically etched GNE with a typical radius of 300 nm is partially insulated to expose only the tip apex (Fig. 1b and Fig. S3). The exposed GNE apex is modified with CB[7]. The typical surface coverage of CB[7] on flat substrate is in the range of 40-50%.^{2, 17, 18} The CB[7] modified GNE is immersed in an electrolyte containing 40 nm diameter GNPs. The potential of the GNE is controlled with respect to an Ag/AgCl reference electrode placed in the bath solution. For some experiments, simultaneous electrochemical measurements are performed at +0.5 V by adding redox mediator ferrocyanide ions in the solution to investigate the GNP collision events.^{16, 19} Upward current spikes are the dominating features in the time-resolved current traces and often last for around one hour (see Fig. S12), suggesting the collision events of GNPs on the CB[7] modified GNE are mainly the ‘hit-n-run’ type.²⁰ When a free moving GNP collides with the GNE, a NPoNE structure containing gold-CB[7]-gold junctions in the nanogap is formed transiently. Fig. 1c illustrates the structure of CB[7] molecular junction in the NPoNE geometry. CB[7] is oriented with its barrel axis perpendicular to the GNE surface.² Total 14 carbonyl groups at the two portals of CB[7] directly interact with both GNE and GNP, facilitating the formation of a NPoNE geometry. The bottom 7 carbonyl groups can bind to gold surface stably after long time deposition, as confirmed by the high stability of CB[7] modified GNPs in various aqueous solution,^{21, 22} single-molecule force spectroscopy,^{17, 23} scanning tunneling microscope (STM) imaging and single-molecule conductance measurements.²⁴ In contrast, due to the limited interaction time, the top 7 carbonyl groups only interact weakly with GNP during the collision events. Therefore, the collision-formed junctions disassemble quickly most of the time. After many collision events, only a few GNPs can stay stably on the GNE surface. One example is shown in the scanning electron microscopy (SEM) image in Fig. 1b inset, which was taken after a regular experiment. The typical number density of adsorbed GNP on the CB[7] modified GNE apex is about 3-5 per μm^2 based on three similar SEM images.

By adding guest molecules in the CB[7] cavity, such as ferrocene (FC) and amino-ferrocene (AFC) shown in the inset of Fig. 1c, the stability of the junctions can be improved, which will be discussed later.

When the tip apex is illuminated with a focused 632.8 nm laser beam, hotspot is formed in the nanogap of the NPoNE structure. Fig. 1d shows the normalized electric field amplitude ($|E/E_0|$) distribution in the center of the nanogap of the NPoNE geometry simulated by Finite-Difference Time-Domain (FDTD) calculation (see Fig. S4). $|E_0|$ is the electric field amplitude of the incident laser. The hotspot area of the NPoNE geometry with electromagnetic enhancement (EME) factor $E_F (\sim |E/E_0|^4) > 10^9$ is about 11.3 nm^2 , which can only cover 2.5 CB[7] molecules assuming the edge-to-edge distance between two neighboring CB[7] molecules is 0.8 nm (half of a CB[7] width), corresponding to a 45% surface coverage of CB[7].

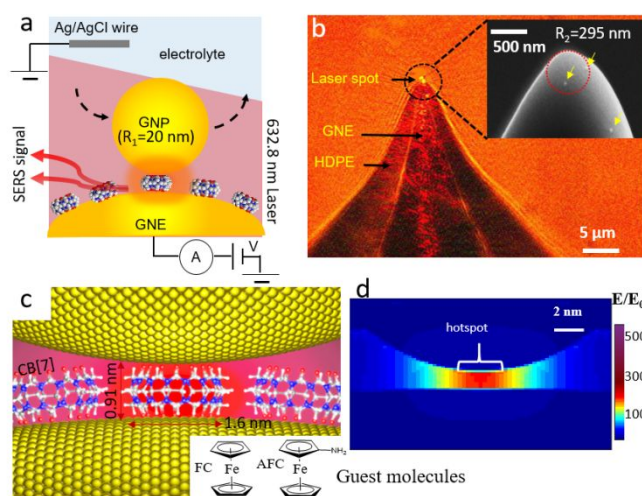


Fig. 1 SERS measurements of CB[7] in a NPoNE junction. (a) A schematic layout of the experimental setup. (b) The optical microscope image of a high-density polyethylene (HDPE) insulated GNE illuminated by a focused laser beam centered at the tip apex (yellow spot) during the SERS experiment. The inset shows a SEM image of a CB[7] modified GNE tip apex after a GNP collision experiment. Three adsorbed GNPs are indicated by the yellow arrows. (c) The illustration of the geometry of a CB[7] plasmonic molecular junction between the GNE and GNP. The atoms in red, blue, grey and white colors are oxygen, nitrogen, carbon and hydrogen atoms, respectively. The inset shows the chemical structure of two guest molecules used in experiments. (d) The FDTD simulation of the normalized electric field amplitude ($|E/E_0|$) distribution in a 0.91 nm nanogap of NPoNE geometry.

Dynamics of transiently formed CB[7] plasmonic molecular junctions.

Before the addition of GNPs in the solution, we observe no detectable SERS signals. After adding GNPs in the solution, SERS signals appear. A time-resolved SERS trajectory with blinking signals is shown in Fig. 2a, which was taken ~60 min after adding GNPs and the GNE was always applied with a +0.5 V bias. The background intensity shows abrupt ‘on’ and ‘off’ within each blinking event, reflecting the transient formation of NPoNE geometry induced by the collision event of a GNP at the exposed GNE surface.²⁵ As shown in the histogrammed lifetime

distribution in Fig. 2b, about 30% of the total blinking events ($N=382$) last less than 51.9 ms (time resolution). The lifetime distribution up to 2 s can be fitted by a single exponential decay function $y = A\exp(-x/t_D)$ (A and t_D are fitting parameters), with the mean lifetime $t_D = 0.12$ s. From the cumulative frequency plot, there are about 6% events with their lifetime longer than 2 s, which cannot be fitted by the single exponential function. They are likely from more stable junctions induced by stronger CB[7]-GNP interactions. The highly fluctuated trajectory often runs for 1-2 hours. This is much different from those observed with 4-Aminothiophenol (4-ATP) or 4-Mercaptobenzoic acid (4-MBA) modified GNEs, where the GNP collision induced blinking signals are less frequent and only appear for a few min before steady Raman signatures of the molecule dominate.^{16, 19} The different phenomenon between molecules reflects the weaker chemical binding force experienced by the colliding GNP from CB[7] than from 4-ATP or 4-MBA. Although most peaks are quite weak in the blinking signals, pronounced peaks often appear in the spectral region between 2100-2200 cm^{-1} , which are shown at the top panel of Fig. 2a in a bigger intensity scale.

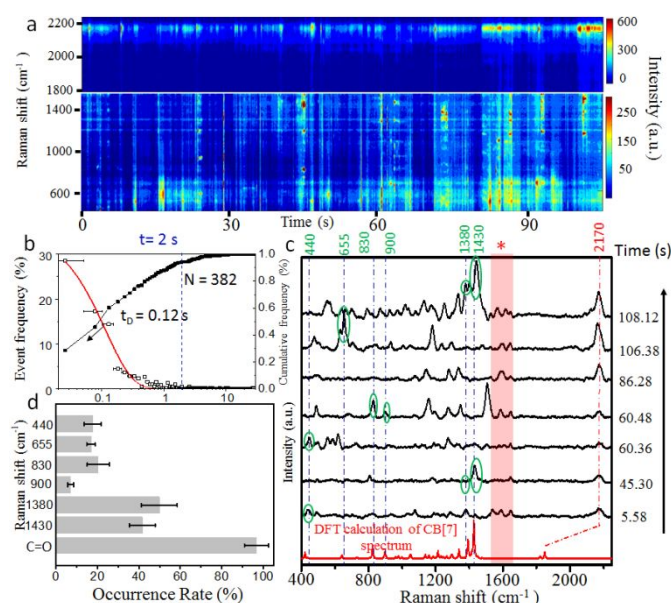


Fig. 2 GNP collision induced blinking events in transiently formed CB[7] NPoNE junctions. (a) The time-resolved SERS trajectory in intensity heat map shows blinking signals. Measurements were carried out in 5 mM phosphate buffer, with 3 mM potassium ferrocyanide and 30 pM GNPs. (b) The histogrammed lifetime distribution (open squares) of 382 blinking events with a bin size 52 ms (shown as error bar). The red line is a fit to data up to 2 s by a single exponential decay function ($R^2=0.97$). The cumulative frequency plot (in solid black dots) is also shown. (c) Transient SERS spectra at different time points from (a) showing the changes of SERS spectra. The characteristic SERS peaks are marked with green circles. Calculated Raman spectrum (red curve) is listed at bottom for comparison. The peaks in the pink shaded region with a "*" are likely from citrate groups. (d) Occurrence frequency of each vibrational mode in the statistics of 382 blinking events. The rate and error are the mean and standard deviation of three measurements, respectively.

Fig. 2c displays the Raman spectra of several fast blinking events (black curves) at different times in the trajectory of Fig. 2a. They show significant variations in the onset of vibrational

peaks. Overall, there are more than 10 frequently appeared peaks, but in each spectrum normally only one or a few peaks appear. It is rare to observe all the peaks in one spectrum and the pattern of the appeared vibrational modes always changes. For the blinking events lasting more than a few frames (each frame takes 51.9 ms), the vibrational modes could also change significantly in the same event. One example is shown in Fig. S5. In the spectral range from 350 cm^{-1} to 1550 cm^{-1} , we can identify six CB[7] peaks (marked with green circles in each spectrum) near 440, 655, 830, 900, 1380 and 1430 cm^{-1} . These are the fingerprint vibrational modes of CB[7] and can match the Raman spectrum of solid sample and the calculated Raman spectrum of CB[7] by density functional theory (DFT) (the red spectrum at the bottom of Fig. 2c). More details can be found in ESI S6 and S7. Their positions are also consistent with the previous reports.²⁶ Several peaks often appear in the range between 1500 and 1640 cm^{-1} , as indicated in the pink shaded region in Fig. 2c. The origin of these peaks is assigned to the vibrational modes of the citrate groups on the GNPs (see supplementary S8). Obviously, the peaks of CB[7] in the range below 1500 cm^{-1} are very weak with the intensities comparable to the major peaks of citrate groups.

Fig. 2d displays the occurrence frequency of seven fingerprint vibrational modes of CB[7] in 382 GNP collision (blinking) events taken from three experiments. The occurrence frequency varies and the symmetric stretching C-N mode at 1380 cm^{-1} and asymmetric stretching C-N mode at 1430 cm^{-1} appear more often. The incomplete and inhomogeneous appearance of the fingerprint modes of CB[7] in each transient spectrum suggests that these signals are likely detected at the single-molecule level. Although we can confirm the formation of CB[7] plasmonic molecular junctions based on these peaks, it is difficult to use these peaks to probe the dynamic changes.

Surprisingly, in the normally silenced spectral range near 2100-2200 cm^{-1} , a few Raman peaks are quite obvious, which appear in most of the blinking events with an occurrence frequency over 90%. After further analysis (in next section), these peaks are determined to be the vibrational modes of C=O groups of CB[7], which directly interact with the colliding GNPs. It is noteworthy that the citrate molecule with three C=O groups may also contribute to this peak, but it appears less frequent and its intensity is much weaker (only ~32% of the main citrate peaks near 1546 cm^{-1}), as suggested by the control SERS experiments (see Fig. S8). In addition, when the citrate molecules on GNPs were replaced by 4-MBA molecules, the prominent peaks in the same spectral range still appear frequently when CB[7] are modified on the GNE surface. Therefore, the observed peak in the range of 2100-2200 cm^{-1} are mainly contributed by the C=O groups of CB[7]. In contrast to the calculated C=O peaks as shown in the red curve of Figure 2c, the experimentally observed C=O peaks in SERS spectra are shifted to a much higher wavenumber. The significant spectral shift could be attributed to the interactions between gold and carbonyl groups of CB[7], as we will discuss below.

Understanding the chemically enhanced C=O peak of CB[7] carbonyl groups.

ARTICLE

Nanoscale

The carbonyl group has a high polarizability, which is sensitive to the nearby atoms and local environment. Therefore, its vibrational frequency appears in a wide range. The typical range of the stretching vibrational mode of C=O bond is from 1600 to 1850 cm^{-1} .²⁷ The spectral range for the metal carbonyl complex is from 1800 to 2200 cm^{-1} .^{28, 29} Based on the molecular structure of CB[7], the electron rich carbonyl group is connected to two electron-donating nitrogen atoms. Therefore, the C=O group of CB[7] has a relatively higher electron density and its bond length (2.1 Å) is shorter than the typical length in ketone. The interaction of carbonyl group with the under-coordinated gold atom of a small gold cluster can also enhance its electron density,³⁰ leading to a higher wavenumber.

We further conducted DFT calculations to understand how the gold-carbonyl interaction affects the C=O Raman peak. As shown in the calculated Raman spectrum in Fig. 2c and Fig. S6.2, there are two peaks corresponding to the collective vibrational modes of all carbonyl groups. The major peak (with a higher wavenumber) of CB[7] is due to the synchronized symmetric vibration of all the carbonyl groups. The minor peak is due to the asynchronized symmetric vibration of all the carbonyl groups (see details in supplementary S6). To reduce the calculation cost, we only investigated the interactions between gold and two carbonyl groups of glycoluril, which is the repeated unit of CB[7]. The model structures are shown in Fig. 3a. Two stable Au₄ clusters are used to represent the gold electrodes. Two C=O peaks are observed for glycoluril, corresponding to the symmetric and asymmetric vibration modes of two carbonyl groups (see details in supplementary S6). Because the asymmetric vibration mode of C=O is further suppressed in CB[7], we will only focus on the major symmetric vibration mode of C=O here. With the approach of the first electrode (Au₄-1), the Au-O distance d_1 is reduced and the C=O symmetric peak is shifted significantly to the higher wavenumber, as shown in the calculated spectra from (i) to (iii) in Fig. 3b. The Mulliken charge analysis reveals that the Au-O interaction induces the CT from gold atom to the oxygen atom and the charge redistribution inside the glycoluril, causing the obvious increase of electron density of the bottom carbonyl group. With the approach of the second electrode (Au₄-2), the electron density of the top C=O bond is also increased because of the CT transfer and charge redistribution. The symmetric C=O peak thus blue shifts again, as shown in spectra (iv) and (v).

The calculations confirm that the $\nu(\text{C}=\text{O})$ peak can be enhanced and blue-shifted due to the gold-to-carbonyl CT. Obviously, the CT is sensitive to the interactions between carbonyl groups and the surface gold atoms of GNP or GNE. Therefore, we can probe the gold-molecule contact dynamics of GNP-CB[7]-GNE junctions by analyzing the spectral and intensity changes of the C=O peak in the SERS spectra. For example in Fig. 2a, the dynamic changes of C=O peak are frequently seen, which are induced by the fast GNP collision events with a 0.5 V bias applied to the GNE. Multiple peaks or a broad peak often appear in the transient spectra between 2100 and 2200 cm^{-1} , reflecting various contact geometries at the gold-CB[7] interfaces triggered by the collisions of GNP with the

GNE surface. After waiting for tens of minutes, the C=O peak becomes stronger and stays near 2172 cm^{-1} with the stable adsorption of a few GNPs on the GNE surface. One example is shown in Fig. 3c. The spectral and intensity fluctuations of C=O peak at 2172 cm^{-1} become smaller. If we removed the free GNPs from the solution, the peak at 2172 cm^{-1} becomes highly stable (Fig. S10), suggesting the Au-carbonyl interaction in the established junction is sensitive to the disturbance by the moving GNPs in the solution.

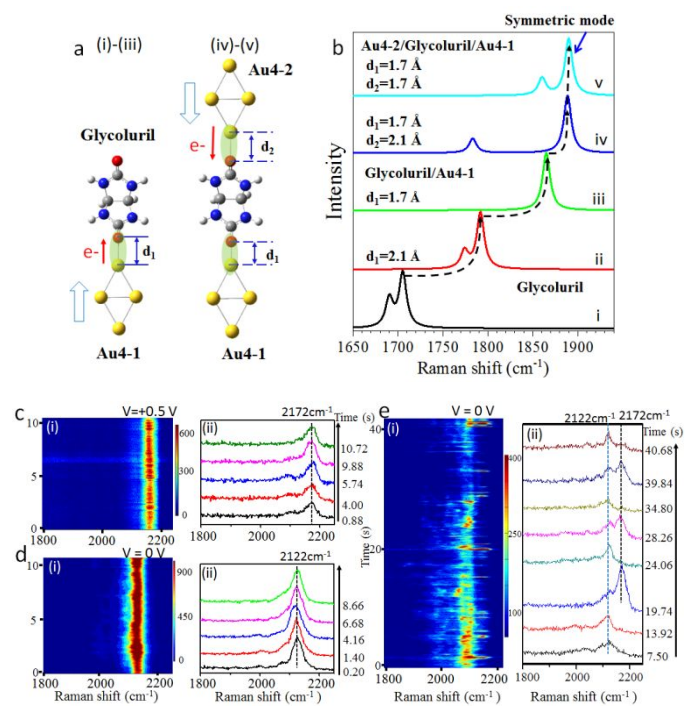


Fig. 3 Dynamics of the C=O vibration peaks. (a) Molecular models for DFT calculations. (b) DFT calculated Raman spectra showing C=O peak changes in five different geometries ((i)-(v)) with zero, one or two Au₄ electrodes. (c-e) (i) A SERS 2D trajectory showing the time-dependent changes of the C=O peak with the applied bias on the GNE at 0.5 V (c), zero bias (d), and after applying +0.5 V to the GNE for a short time and recorded at zero bias (e). (ii) A few spectra from (i) at different time points. GNPs are added in the solution for all the experiments.

Interestingly, the gold-CB[7] contact can also be regulated by the applied bias on the GNE. Fig. 3d shows the stable C=O peak from the self-assembled NPoNE geometries when the GNE was kept at zero bias until the C=O peak is stabilized. Compared with the stable spectra at +0.5 V in Fig. 3c, the peak position is down-shifted to 2122 cm^{-1} . The down shift of the C=O peak position suggests the charge transfer from gold to the C=O bond is reduced due to the weaker Au-O interaction at zero bias. In addition, bigger fluctuations in both intensity and frequency are observed for the C=O peak at zero bias, attributing to the reduced junction stability as a consequence of the weaker Au-O interactions. To further test the bias effect, we applied a positive bias (+0.5 V) for a short time (~ 2 min) to the GNE and then changed it to zero bias. Interestingly, transient switching

signals from 2122 cm^{-1} to 2172 cm^{-1} appear in the trajectory (see Fig. 3e(i)). The two peaks at both 2122 cm^{-1} and 2172 cm^{-1} can be clearly observed in the selected transient spectra in Fig. 3e(ii). At a later time, the C=O peak settles again near 2122 cm^{-1} at zero bias. We have demonstrated previously^{16, 19} that the positive bias applied on the GNE can slightly push the adsorbed negatively charged GNP toward the GNE surface. The compressive force can improve the electronic coupling of the gold-carbonyl interaction and benefit the CT, leading to the blue shift of C=O peak.

Probing the dynamics of the complexed CB[7] cavity.

We further study the dynamics of the junctions when complexed CB[7] is introduced in the NPoNE geometry. Herein, we focus on FC and a FC derivative AFC, and study their molecular behaviour in the complexed state with CB[7] (AFC@CB[7] and FC@CB[7]) in the NPoNE geometry. The AFC@CB[7] and FC@CB[7] host-guest complexes are preformed in solution prior to the GNE modification (see ESI S1). FC is known to form strong 1:1 host-guest complexes with CB[7], with the equilibrium binding affinity $\log K = 5.6$.³¹ The binding affinity between AFC and CB[7] is even higher due to additional interactions between amine and carbonyl groups.^{32, 33} In our measurements, we find the SERS signals of the FC@CB[7] are weaker and less stable than those of AFC@CB[7]. Therefore, we mainly focus on the analysis of the AFC@CB[7] results.

With the presence of GNPs in the solution, blinking signals are again observed in the recorded SERS trajectories. One example of the blinking signal is shown in Fig. 4a. The blinking only occurs in the spectral range below 1550 cm^{-1} and the pronounced C=O peak is relatively stable. Typically, the C=O peak became stable in less than 10 min, suggesting the GNPs can be adsorbed faster to the AFC@CB[7] modified GNE surface than to the CB[7] modified GNE. In addition, we did not observe obvious bias-dependent spectral shift of the C=O peak for these complexed systems, and the C=O peak could quickly stabilize even at zero bias. These are quite different from the SERS results of CB[7]. As reported in the dynamic STM-break junction measurement,³⁴ the C_p rings of confined FC or AFC in the CB[7] cavity can form reliable van der Waals interactions with gold. The extra gold-guest interactions enhance the stability of AFC@CB[7] and AFC@CB[7] molecules on the GNE surface, therefore improving the GNP residence on the GNE and increasing the lifetime of the formed NPoNE junctions, compared with the counterparts of CB[7]-only junctions. Because the carbonyl-Au interaction is stable, the blinking signals observed here should come from the fluctuations inside the established junctions formed by the adsorbed GNPs, rather than from the dynamic formation of junctions during the GNP collision events.

In the blinking events, the vibrational peaks below 1550 cm^{-1} also vary significantly between the spectra. The spectra (in black color) of two representative fast blinking events 3 and 4 (lasting for only 1 frame) are shown in Fig. 4b. Only one major peak appears in each spectrum in the range below 1550 cm^{-1} . The average spectrum of 10 such transient spectra is displayed in red color, where three weak Raman peaks of CB[7] at 830, 1380

and 1430 cm^{-1} (marked with green arrows) can be identified. This new peak is from AFC, which will be discussed in following paragraphs. Peaks due to citrate molecules are also identified in the spectra, which are mainly in the range of $1500\text{--}1640\text{ cm}^{-1}$.

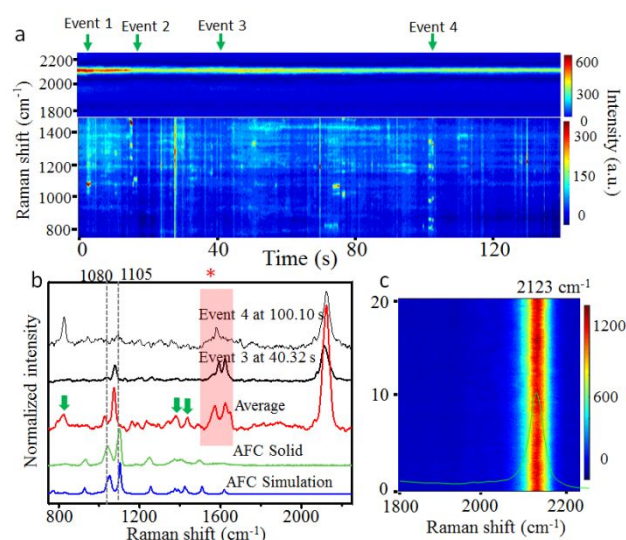


Fig. 4 SERS spectra of AFC@CB[7] plasmonic junctions. (a) A typical time-resolved SERS trajectory acquired in the presence of 30 pM GNPs in solution with an AFC@CB[7] functionalized GNE. The bias is +0.5 V. (b) Two representative Raman spectra from two fast blinking events in the SERS trajectory of Figure 4a (black). The red color curve is the averaged spectrum of 10 similar transient spectra. For comparison, the Raman spectrum of solid sample (green) and DFT calculated Raman spectrum of AFC (blue) are listed at the bottom. (c) A typical SERS trajectory shows the stable C=O peak. The time-average spectrum (green color) is superposed on top of the heatmap.

The mean position of the C=O peak is at about 2123 cm^{-1} (Fig. 4c), which is shifted to the lower wavenumber compared with the case of stable CB[7] junction at 0.5 V. The included guest molecule might induce charge redistribution in the CB[7] molecule and affect the charge transfer between carbonyl groups and gold atoms, which results in the down-shift of the C=O peak. In measurements of FC@CB[7], the C=O peak mainly appears near 2150 cm^{-1} , which is slightly higher than that of AFC@CB[7] (Fig. S6.2).

The blinking events with a longer lifetime provide us with opportunities to study the dynamic changes in the AFC@CB[7] plasmonic nanojunction. The dynamic change of the new peak near 1080 cm^{-1} is the most noticeable. The trajectories (i) and (ii) of Fig. 5a are the zoom-in of two longer lived events, corresponding to events 1 and 2 in the trajectory shown in Fig. 4a. In (i), the peak at 1080 cm^{-1} suddenly appears and lasts for less than 2 s. The trajectory (ii) also shows the sudden appearance of peak 1080 cm^{-1} , which shifts to 1105 cm^{-1} before its disappearance. Fig. 5a (iii) shows the switching between 1080 and 1105 cm^{-1} . For this example, there is no free-moving GNP in the solution. In all three cases, the C=O is relatively stable, suggesting the GNP is stable on the GNE surface. The observed dynamic changes should be mainly due to the changes

of both gold adatom and the guest molecule at the gold-AFC interface.

The new peak at 1080 cm^{-1} (or 1105 cm^{-1}) is assigned to the cyclopentadienyl (C_p) ring breathing mode, which has been previously reported for the SERS measurements of GNP aggregates⁷ and NPoM junctions.⁶ However, Raman spectra of AFC powders (green color in Fig. 4b) and DFT based calculations of AFC (blue color) in gas phase both show that the C_p ring breathing mode is peaked at $\sim 1105\text{ cm}^{-1}$. There is about 25 cm^{-1} down-shift when the AFC@CB[7] complex is inside the NPoNE geometry. Similar down shift of C_p ring breathing mode peak is also observed for the FC@CB[7] complex in the NPoNE geometry. According to the previous reports, no shift was observed in the Raman spectra of solid powder of FC@CB[7].³⁵ This is consistent with our DFT calculations for both FC@CB[7] and AFC@CB[7] complexes (see Fig. S6.1). So the down shift of 1105 cm^{-1} peak observed in our experiments is not due to the complexation of AFC inside the CB[7] cavity. Regarding the mechanism of the downshifts, we propose that they are attributed to the charge transfer induced by the interaction between surface gold atoms and the C_p rings of FC or AFC molecules confined in the CB[7] cavity.

To investigate the charge transfer mechanism, we carried out DFT calculations of FC and AFC in a gold nanogap formed by two structurally stable Au₂₀ clusters. Since FC or AFC may have two orientations inside the CB[7] cavity and the reactivity of surface gold atom varies, we have calculated a series of Au₂₀-molecule-Au₂₀ geometries with different orientations of molecule and Au₂₀ clusters (see Fig.S6.3a). Four selected geometries are shown in Fig.5b to show the molecular orientation effect and to compare the difference between AFC and FC. In the horizontal orientation (1), the main axis of FC molecule (intersecting the centers of two C_p rings) is almost perpendicular to the main axis of CB[7]. In the vertical orientation (6), the main axis of FC is parallel with the main axis of CB[7]. Based on the energy analysis, FC is more stable at the horizontal orientation in the CB[7] cavity when no gold nanogap is involved. This is consistent with the X-ray crystal structure of FC@CB[7].³³ However, when positioned in the nanogap between gold electrodes, FC becomes more stable at a vertical orientation due to the additional interactions between the C_p rings and the gold atoms.³⁴ Therefore, the FC molecule is expected to stay mainly in a vertical orientation when the FC@CB[7] is in the NPoNE junction. This is essentially the same for AFC. We have calculated the interaction energy between Au₂₀ cluster and FC (or AFC) in 8 different Au₂₀-molecule configurations (Fig. S6.4). The strongest interactions happen when the Au₂₀ tip points to the C_p ring center. Fig.5b shows the two nanojunction configurations with the strongest molecule-metal interactions for FC (6) and AFC (7), with FC and AFC in the vertical orientation and the surface gold atoms are under-coordinated. The higher interaction energy leads to a higher stability of the junction.

We examined the charge distribution for all 8 nanojunction configurations (Table S2). The two most stable configurations 6 and 7 also show the most effective molecule-to-metal CT and the largest charge redistribution across the whole complex,

suggesting the strongest electronic coupling. The gold tip withdraws more partial electron from the interacting C_p ring than the case of gold flat surface, which is attributed to the higher reactivity of the under-coordinated gold atoms. The molecule-to-metal CT process often leads the shift of the vibrational peak of C_p ring to a lower wavenumber. As shown in the calculated Raman spectra in Fig. 5c, the C_p ring breathing mode peaks of both configurations 6 and 7 show the biggest down-shift from 1105 cm^{-1} to near 1080 cm^{-1} , which matches the experimental results. Therefore, the configurations 6 and 7 are likely to be the most observable configurations in our experiments.

We find that the Au₂₀ tip interacts stronger with the C_p ring of AFC than FC. The amine group of AFC is an electron donating group (EDG) for the C_p ring. Compared with FC, both C_p rings of AFC show increased electron density (Table S2), resulting in the stronger interactions with the gold electrode. This is consistent with the experimental observations of the more stable spectra of AFC@CB[7] junctions in SERS measurements and the higher magnitude and longer duration of current spikes in the EC current measurements (Table S4).

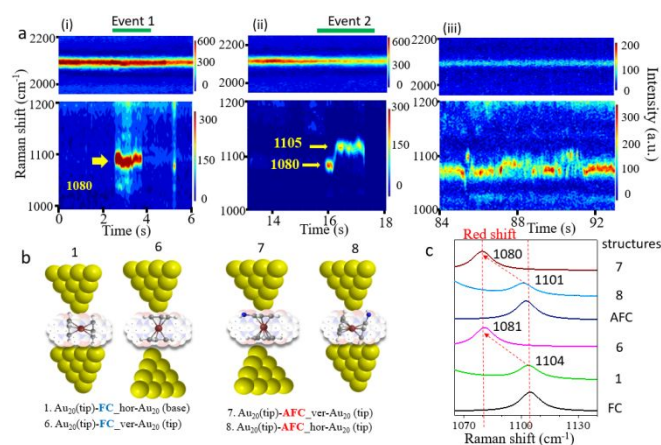


Fig. 5 Dynamics of guest molecule AFC in the AFC@CB[7] plasmonic junctions. (a) (i-ii) The zoom-in of events 1 (i) and 2 (ii) in the trajectory of Figure 4a. (iii) A short SERS trajectory with switching between 1080 cm^{-1} and 1105 cm^{-1} . Measurements were carried out with GNPs in the solution. (b) Four selected DFT simulation configurations with FC and AFC in vertical and horizontal orientations between two Au₂₀ clusters, representing GNP and GNE. The other configurations are showed in Fig. S6.3a. (c) The calculated Raman peak of the C_p breathing vibrational mode in the four selected configurations. The spectra of free FC and AFC are also added for comparison. The spectra of other configurations are showed in Fig. S6.3b.

In control experiments of only AFC or FC modified GNEs, we did not observe the strong C_p peak in the SERS spectra, attributing to the very low coverage of AFC or FC on the GNE (Fig. S2.1). Therefore, the spectral change of the C_p ring breathing mode can be exploited as an internal reference to interpret the dynamic changes of guest molecule AFC inside the CB[7] cavity. The presence of strong C_p ring breathing mode peak in the three events of Fig. 5a suggests the complexed AFC@CB[7] is in the NPoNE junctions. The spectral shift to 1080

cm^{-1} is attributed to the CT based CE, induced by the stronger interaction between C_p ring and the surface gold adatoms. The stronger interaction may create or draw a mobile gold adatom to settle near the C_p ring center, forming a 'picocavity' type hotspot³⁶ and causing the sudden burst of 1080 cm^{-1} peak. The transitions between 1080 and 1105 cm^{-1} in examples (ii) and (iii) of Fig. 5a are likely induced by the rotation motions of the AFC guest molecule in the CB[7] cavity. Although the AFC is mainly in the vertical orientation when it is confined in the CB[7] cavity of the NPoNE geometry, it also has chances to rotate to the horizontal orientation, leading to the sudden appearance of the 1080 cm^{-1} peak. The rotation motion of AFC may also be triggered by the thermal fluctuation of the interacting gold adatom.

2D Correlation analysis and principal component analysis

To better understand the dynamic and complex SERS data, we have carried out two-dimensional correlation spectroscopy (2D COS) analysis of the time-resolved SERS results. The 2D correlation contour maps of CB[7] junction (Fig. 6a) and AFC@CB[7] junction (Fig. 6b) were constructed from the blinking data of Fig. 2a and Fig. 4a, respectively. The major peaks of CB[7] before 1500 cm^{-1} can be identified in the 2D correlation map but they are generally weak. This is consistent with their low intensity in the spectra (see Fig. 2c). Among them, the peak near 1430 cm^{-1} shows a relatively high intensity. The carbonyl group signal between 2100 and 2200 cm^{-1} is the most prominent signal in the map, suggesting the high intensity of this peak in experiments. The carbonyl peak also has positive correlation with all other peaks, including both the CB[7] peaks and the citrate peaks near 1600 cm^{-1} . These results confirmed that most of the blinking changes in the SERS time traces are from the GNP collision events, which can enhance all the vibrational modes in the transiently formed hotspot through electromagnetic enhancement and produce correlated changes. These results also reflect the carbonyl group of CB[7] is highly sensitive to the junction dynamic formation and deformation process and can be further enhanced by chemical enhancement. In addition, the prominent C_p ring peaks only appear in the map of AFC@CB[7] junction but not in the map of CB[7] junction. The C_p peak mainly appears near 1080 cm^{-1} instead of 1105 cm^{-1} .

We also performed principal component analysis (PCA) on CB[7] and AFC@CB[7] data. The loading plots are shown in Fig. 6c and d. The first four principal components (PC1, PC2, PC3 and PC4) only account for 68.4% variation of CB[7] (Fig. S13a) and 59.1% variation of AFC@CB[7] (Fig. S13b). The low percentage is originated from the incomplete and highly variable transient spectra induced by the dynamic collision events (see Fig. 2c and Fig. 4b). Due to the generally longer lifetime of each AFC@CB[7] event, the spectral differences between events become more obvious, leading to the lower percentage of variation for PCs of AFC@CB[7]. The PC1 of CB[7] shows 811 , 1440 and 2170 cm^{-1} peaks, corresponding to the CB[7]'s vibration modes. The PC1 of AFC@CB[7] presents the obvious changes near 1080 and 2123 cm^{-1} , corresponding to the AFC C_p ring

breathing and Carboxyl modes. It is obvious that the PCA scores spread out in the scatter plots (see Fig. S13 c-d), further revealing the inhomogeneity between all the blinking spectra.

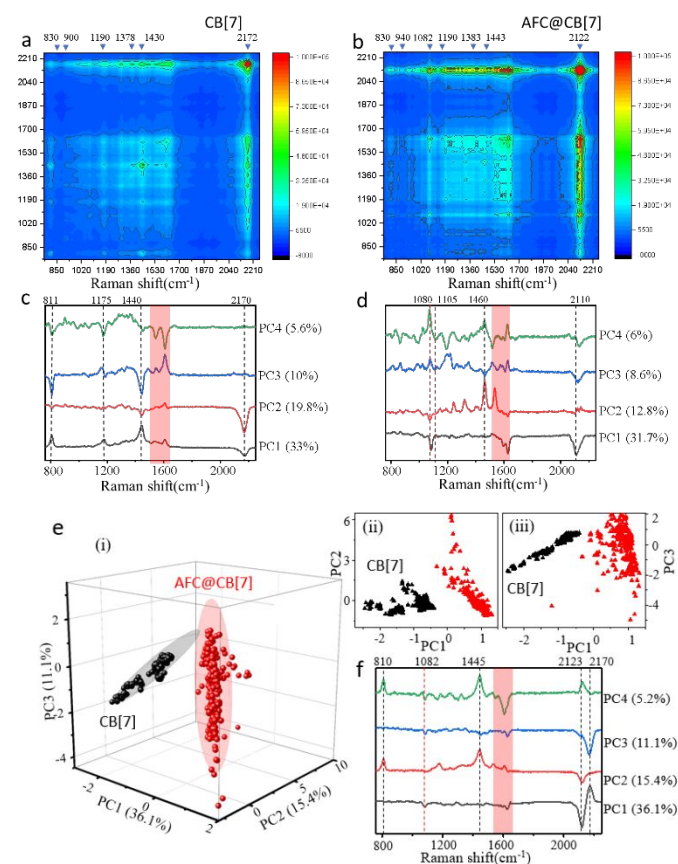


Fig. 6 2D-COS analysis and PCA of the time-resolved SERS data of CB[7] and AFC@CB[7]. (a-b) The synchronous 2D-COS contour map of CB[7] (a) and AFC@CB[7] (b). (c-d) The loading plots of the first four PCs for CB[7] (c) and AFC@CB[7] (d). The pink shaded regions show the contribution from citrate peaks. (e) (i) The distribution of PCA scores of the clustered data for CB[7] (red dots) and AFC@CB[7] (black dots) under the first three PCs. The shaded Ellipse area are 95% confidence range for each cluster. (ii-iii) The projected PCA scatter plots on the PC1-PC2 and PC1-PC3 planes. (f) The corresponding loading plots for the mixed CB[7]-AFC@CB[7] data.

To further explore the differences between the SERS data of CB[7] and AFC@CB[7], a new PCA analysis was carried out on the combined data of CB[7] and AFC@CB[7]. From the 3D and 2D scatter plots of PCA (Fig. 6e (i)-(iii)), we can see that CB[7] and AFC@CB[7] data form two distinguishable clusters. The first four PCA loading plots are shown in Fig. 6f. They account for 36.1%, 15.4%, 11.1%, and 5.2% of the total variance, respectively. The most significant differences between CB[7] and AFC@CB[7] are rising from the carbonyl peak at 2123 cm^{-1} of AFC@CB[7] and 2170 cm^{-1} of CB[7], as shown in the loading plot of PC1. The contribution of C_p ring breathing mode can also be observed around 1080 cm^{-1} in PC1. Therefore, The shift of carbonyl and new C_p peak contribute significantly to the difference between CB[7] and AFC@CB[7]. The loading plot of PC2 shows obvious CB[7] peaks at 810 , 1445 and 2123 cm^{-1} , revealing the variations of CB[7] peaks induced by the host-guest interactions.

In summary, plasmonic molecular junctions containing CB[7] and its host-guest complexes in NPoNE geometries are self-assembled by GNP collision events, and are probed by time-resolved SERS. New chemically enhanced vibrational modes have been identified as signature peaks in the SERS spectra for the dynamic studies. The enhancement of these peaks is attributed to the metal-molecule CT by specific gold-molecule interactions with both host and guest molecules. Pronounced CB[7] C=O vibration peaks are observed in the spectral range 2100-2200 cm^{-1} , which are selectively enhanced due to the gold-carbonyl interaction at the metal-molecule interfaces as revealed by the DFT calculations. The C=O vibration peaks are highly distinguishable because they are strong and well separated from the crowded spectral range below 1550 cm^{-1} . Importantly, the C=O peak is very sensitive to small changes at the CB[7]-gold interfaces in the plasmonic junction. Large dynamic spectral changes of C=O peak are observed in the time-resolved SERS trajectories, triggered by the GNP collision events or modulated by the applied bias to the GNE. With the applied positive bias, the Au-carbonyl interaction can be strengthened and the CB[7] junction can be stabilized. Interestingly, with the inclusion of guest molecule AFC or FC in the CB[7] cavity, the junction becomes more stable, as confirmed by the quickly stabilized C=O peak. This may be attributed to the extra metal-guest molecule interactions, which also induce the new stable orientation of AFC or FC inside the CB[7] cavity. Because of the strong interaction between C_p ring and gold adatoms, the Raman peak of C_p ring of guest molecule AFC or FC becomes prominent. Based on the position shift and intensity change of this peak, the rotational motion of the confined AFC inside CB[7] cavity is revealed.

Together with DFT simulations and statistical analysis, this report provides new insights into the mechanism of a few less-studied surface-enhanced Raman peaks in the metal-CB[n]-metal junctions. Because various guest molecules can be included in the cavity of CB[n], these better-understood peaks could serve as powerful SERS probes to resolve the dynamics of gold-CB[n] interactions, host-guest interactions, guest-guest interactions and reactions at single molecule level, which will benefit the studies of chemistry under nanoconfinement, molecular electronics, heterogeneous catalysis, biosensing and drug delivery applications.

Experimental

GNE fabrication and chemical modification. The GNEs were fabricated as described in previous reports.^{16, 37} Briefly, a gold wire was electrochemically etched and insulated with HDPE to expose only the tip apex. After cleaning, it was immersed in a molecular solution for chemical modification. Full details of GNE fabrication and characterization are described in Supplemental information S3. The immobilizations of CB[7], FC@CB[7] and AFC@CB[7] on the gold substrates have been investigated by electrochemical measurements and FTIR spectroscopy (see Supplemental information S2).

SERS measurements. Raman spectroscopy was performed on a Nikon Ti-U microscope-based setup, as described previously. The spectra were collected with a CCD camera (PIXIS 100B_eXcelon, Princeton Instrument) with a spectral resolution of $\sim 2 \text{ cm}^{-1}$. Each spectrum was acquired with a time resolution of 51.9 ms (50 ms CCD integration time and 1.9 ms CCD readout time), and we typically collected 1000 to 2000 spectra continuously for each SERS trajectory measurement. The power of 632.8 nm laser was attenuated by ND filters to 1.35 mW and focused at the GNE apex. The power density was about 0.047 $\text{mW}/\mu\text{m}^2$ based on the typical laser spot radius 3 μm . The GNE was placed in a liquid cell containing 5 mM phosphate buffer solution (PBS, pH = 7.4). In some experiments, Potassium Ferrocyanide was added with a concentration of 3 mM for electrochemical current measurements. We did not notice any differences in the SERS spectra induced by the redox mediator. The concentration of 40 nm GNPs was 30 μM . All the measurements were performed at room temperature. The SERS results were analyzed with custom LabView (National Instruments) and Matlab (MathWorks Inc.) programs.

FDTD simulation and DFT calculations. FDTD simulations were carried out by using a commercial software package (Lumerical Solutions, Inc.) to calculate the electric field distribution in the hotspot of GNP-on-GNE structures. The details are given in the Supplemental information S4. DFT calculations of the Raman spectrum were carried out with GAUSSIAN 16 software package. The structures were optimized using the built-in molecular mechanics and the DFT calculations of these structures were performed at their ground-state equilibrium geometry conformation using hybrid exchange–correlation functional (B3LYP) with Coulomb-attenuating method (CAM) (see Supplementary information S6).³⁸ Au₄ and Au₂₀ clusters were used to represent the gold electrodes. The calculated Raman spectra were plotted by applying a Lorentzian function with a full-width at half-height (FWHM) of 20 cm^{-1} . We also used the DFT-D3 method for dispersion correction when calculating the host-guest complexes with or without the gold cluster.

Conflicts of interest

There are no conflicts to declare.

Acknowledgements

This work was partially supported by the Engineering Research Centers Program of the National Science Foundation under NSF Cooperative Agreement No. EEC-1647837 (J.H.), NSFC (21705122 for S.C. and 21372183 for F.L.), and the Program for Innovative Teams of Outstanding Young and Middle-aged Researchers in the Higher Education Institutions of Hubei Province (T201702 for F.L.). We acknowledge the computing resources provided by the Instructional & Research Computing Center (IRCC) at Florida International University.

Notes and references

1. J. Lagona, P. Mukhopadhyay, S. Chakrabarti and L. Isaacs, *Angew. Chem. Int. Ed.*, 2005, **44**, 4844.
2. Q. An, G. Li, C. Tao, Y. Li, Y. Wu and W. Zhang, *Chem. Commun.*, 2008, 1989.
3. A. B. Zrimsek, N. Chiang, M. Mattei, S. Zaleski, M. O. McAnally, C. T. Chapman, A.-I. Henry, G. C. Schatz and R. P. Van Duyne, *Chem. Rev.*, 2017, **117**, 7583.
4. S. Nie, *Science*, 1997, **275**, 1102.
5. K. Kneipp, Y. Wang, H. Kneipp, L. T. Perelman, I. Itzkan, R. Dasari and M. S. Feld, *Phys. Rev. Lett.*, 1997, **78**, 1667.
6. D. O. Sigle, S. Kasera, L. O. Herrmann, A. Palma, B. de Nijs, F. Benz, S. Mahajan, J. J. Baumberg and O. A. Scherman, *J. Phys. Chem. Lett.*, 2016, **7**, 704.
7. C. A. Tao, Q. An, W. Zhu, H. Yang, W. Li, C. Lin, D. Xu and G. Li, *Chem. Commun.*, 2011, **47**, 9867.
8. R. W. Taylor, T.-C. Lee, O. A. Scherman, R. Esteban, J. Aizpuru, F. M. Huang, J. J. Baumberg and S. Mahajan, *ACS Nano*, 2011, **5**, 3878.
9. S. L. Kleinman, R. R. Frontiera, H. Anne-Isabelle, J. A. Dieringer and R. P. Duynne, Van, *Phys. Chem. Chem. Phys.*, 2012, **15**, 21.
10. J. Reguera, J. Langer, D. Jimenez de Aberasturi and L. M. Liz-Marzan, *Chem. Soc. Rev.*, 2017, **46**, 3866.
11. X. Xiao and A. J. Bard, *J. Am. Chem. Soc.*, 2007, **129**, 9610.
12. C. M. Hill, J. Kim and A. J. Bard, *J. Am. Chem. Soc.*, 2015, **137**, 11321.
13. F. T. Patrice, K. Qiu, Y. L. Ying and Y. T. Long, *Annu. Rev. Anal. Chem.*, 2019, **12**, 347.
14. P. K. Aravind, R. W. Rendell and H. Metiu, *Chem. Phys. Lett.*, 1982, **85**, 396.
15. C. Ciraci, R. T. Hill, J. J. Mock, Y. Urzhumov, A. I. Fernandez-Dominguez, S. A. Maier, J. B. Pendry, A. Chilkoti and D. R. Smith, *Science*, 2012, **337**, 1072.
16. J. Guo, J. Pan, S. Chang, X. Wang, N. Kong, W. Yang and J. He, *Small*, 2018, **14**, e1704164.
17. A. Gomez-Casado, P. Jonkheijm and J. Huskens, *Langmuir*, 2011, **27**, 11508.
18. D.-W. Lee, K. M. Park, B. Gong, D. Shetty, J. K. Khedkar, K. Baek, J. Kim, S. H. Ryu and K. Kim, *Chem. Commun.*, 2015, **51**, 3098.
19. T. Ma, J. Guo, S. Chang, X. Wang, J. Zhou, F. Liang and J. He, *Phys. Chem. Chem. Phys.*, 2019, **21**, 15940.
20. W. Wang and N. Tao, *Anal. Chem.*, 2013, **86**, 2.
21. Y. Han, X. Yang, Y. Liu, Q. Ai, S. Liu, C. Sun and F. Liang, *Sci. Rep.*, 2016, **6**, 22239.
22. P. Xu, Q. Feng, X. Yang, S. Liu, C. Xu, L. Huang, M. Chen, F. Liang and Y. Cheng, *Bioconjugate Chem.*, 2018, **29**, 2855.
23. M. Zhang, Z. Gong, W. Yang, L. Jin, S. Liu, S. Chang and F. Liang, *ACS Appl. Nano Mater.*, 2020, **3**, 4283.
24. B. Xiao, F. Liang, S. Liu, J. Im, Y. Li, J. Liu, B. Zhang, J. Zhou, J. He and S. Chang, *Nanotechnology*, 2018, **29**, 365501.
25. S. Mahajan, R. M. Cole, J. D. Speed, S. H. Pelfrey, A. E. Russell, P. N. Bartlett, S. M. Barnett and J. J. Baumberg, *J. Phys. Chem. C*, 2010, **114**, 7242.
26. S. Mahajan, T.-C. Lee, F. Biedermann, J. T. Hugall, J. J. Baumberg and O. A. Scherman, *Phys. Chem. Chem. Phys.*, 2010, **12**, 10429.
27. R. M. Silverstein, G. C. Bassler and T. C. Morrill, *Spectrometric identification of organic compounds*, Wiley, New York, 5th edn., 1991.
28. K. V. Kong, Z. Lam, W. K. O. Lau, W. K. Leong and M. Olivo, *J. Am. Chem. Soc.*, 2013, **135**, 18028.
29. F. A. Cotton and C. S. Kraihanzel, *J. Am. Chem. Soc.*, 1962, **84**, 4432.
30. G. S. Shafai, S. Shetty, S. Krishnamurthy, V. Shah and D. G. Kanhere, *The Journal of Chemical Physics*, 2007, **126**, 014704.
31. W. Ong and A. E. Kaifer, *Organometallics*, 2003, **22**, 4181.
32. S. Liu, C. Ruspic, P. Mukhopadhyay, S. Chakrabarti, P. Y. Zavalij and L. Isaacs, *J. Am. Chem. Soc.*, 2005, **127**, 15959.
33. W. S. Jeon, K. Moon, S. H. Park, H. Chun, Y. H. Ko, J. Y. Lee, E. S. Lee, S. Samal, N. Selvapalam, M. V. Rekharsky, V. Sindelar, D. Sobransingh, Y. Inoue, A. E. Kaifer and K. Kim, *J. Am. Chem. Soc.*, 2005, **127**, 12984.
34. M. Huang, M. Sun, X. Yu, S. He, S. Liu, W. M. Nau, Y. Li, T. Wu, Y. Wang, S. Chang and J. He, *J. Phys. Chem. C.*, 2020, DOI: 10.1021/acs.jpcc.0c02411.
35. Y. Chen, A. Klimczak, E. Galoppini and J. V. Lockard, *RSC Adv.*, 2013, **3**, 1354.
36. F. Benz, M. K. Schmidt, A. Dreismann, R. Chikkaraddy, Y. Zhang, A. Demetriadou, C. Carnegie, H. Ohadi, N. B. De and R. Esteban, *Science*, 2016, **354**, 726.
37. M. Tuchband, J. He, S. Huang and S. Lindsay, *Rev. Sci. Instrum.*, 2012, **83**, 015102.
38. T. Yanai, D. P. Tew and N. C. Handy, *Chem. Phys. Lett.*, 2004, **393**, 51.

TOC

SERS is combined with electrochemical single-entity technique to probe the dynamic molecular changes in the transiently formed gold-CB[7]-gold junctions

